

Probing Cosmic Origins with CO and [CII] Emission Lines

Azadeh Moradinezhad Dizgah,^{1,*} Garrett K. Keating,² and Anastasia Fialkov²

¹*Department of Physics, Harvard University, 17 Oxford St., Cambridge, MA 02138, USA*

²*Harvard-Smithsonian Center for Astrophysics, 60 Garden Street, Cambridge, MA 02138, USA*

Primordial non-gaussianity (PNG) is an invaluable window into the physical processes that gave rise to cosmological structure. The presence of local shape PNG imprints a distinct scale-dependent correction to the bias of dark matter tracers on large scales, which can be effectively probed via the technique of intensity mapping. Considering an upcoming generation of experiments, we demonstrate that intensity mapping of CO and [CII] emission can improve upon the current best constraints from the Planck satellite. We show that measurement of the CO intensity power spectrum by a hypothetical next stage of the ground-based COMAP experiment can achieve $\sigma(f_{\text{NL}}^{\text{loc}}) = 3.7$, and that the proposed CMB satellite mission PIXIE can achieve $\sigma(f_{\text{NL}}^{\text{loc}}) = 4.9$ via measurement of [CII] intensity power spectrum.

PACS numbers:

Introduction: Understanding the origin of structure in the Universe is a key open question in cosmology. Inflation [1–3] is the leading paradigm of the early Universe, in which quantum fluctuations of a scalar field, i.e. inflaton, planted the seed for the formation of the structure [4–7]. The simplest models of inflation, characterized by a canonical single scalar field, originating from the Bunch-Davies vacuum and slowly rolling down its potential, predict a nearly Gaussian distribution of primordial perturbations [8–10]. Deviations from these simple models can produce a distinctive, non-Gaussian signature which, to leading-order, results in non-zero bispectrum of primordial curvature perturbations ζ (see [11, 12] for reviews). It is common to write the bispectrum in terms of a scale-independent amplitude f_{NL} and a shape function; constraint on this amplitude (for a given shape) is a unique probe to discriminate between models of inflation.

PNG of the local shape [10, 13–15], which is produced by super-horizon, non-linear evolution of ζ , can be parametrized by a non-linear correction to the Gaussian perturbations ζ_G , as $\zeta = \zeta_G + 3/5 f_{\text{NL}}^{\text{loc}} (\zeta_G^2 - \langle \zeta_G^2 \rangle)$. The local shape PNG is a sensitive probe of multi-field inflation, as single-field scenarios, in the attractor regime, are expected to produce $f_{\text{NL}}^{\text{loc}} \ll 1$ [16, 17]. Current best constraints on $f_{\text{NL}}^{\text{loc}}$ are set by measurements of the cosmic microwave background (CMB) from the Planck satellite [18]. These results are consistent with Gaussian primordial fluctuations ($f_{\text{NL}}^{\text{loc}}=0$), with a $1-\sigma$ uncertainty – when translated to large-scale structure (LSS) conventions – of $\sigma(f_{\text{NL}}^{\text{loc}}) \simeq 6.5$ [19]. These constraints can be significantly improved by measurements of the statistical properties of LSS (see [20] for an overview). Among other effects, PNG leaves an imprint on the power spectrum of biased tracers of dark matter by inducing a scale-dependent correction to their bias, which is significant on large scales [21–23]. In this Letter, we show that with this signature, power spectrum measurements from intensity mapping of CO and [CII] line emission have the potential to improve the constraints on PNG beyond the current best limits.

In contrast to galaxy surveys, which aim to detect groups of individual sources to some threshold significance and completeness, line intensity mapping probes the large-scale matter distribution by measuring the cumulative light from an ensemble of sources, including faint, unresolved galaxies, while preserving accurate redshift information. Previous studies have shown that intensity mapping of the 21-cm line of neutral hydrogen (HI) at redshifts $z = 1 - 5$, with purpose-designed surveys, can produce constraints of order $\sigma(f_{\text{NL}}^{\text{loc}}) \sim 1$ [24]. Interest in other emission lines as candidates for intensity mapping has been bolstered by the tentative power spectrum detections of CO and [CII] [25, 26], and the multitude of upcoming intensity mapping surveys (see [27] for a recent summary). Here, we provide the first forecast for the potential of such surveys in constraining PNG, considering experimental setups targeting CO and [CII] emission from as far back in time as the Epoch of Reionization (EoR; $z \sim 6-10$), mapping the cosmic web at redshifts and scales that are inaccessible to upcoming spectroscopic/photometric galaxy surveys.

The line intensity power spectrum: CO is predominantly found in the dense clouds of molecular gas (of density $n \sim 10^3 \text{ cm}^{-3}$), while [CII] is found in the neutral media of galaxies ($n \sim 1 \text{ cm}^{-3}$) [28]. Both are typically tracers of the cold gas within galaxies that provide the fuel for star formation, and the strength of their emission is observed to be correlated with the star formation rates of galaxies [29, 30]. Under the assumption that line emission for both CO and [CII] arise primarily from within galaxy host halos, and that the luminosities of these lines can be expressed as a function of halo mass, the mean brightness temperature (typically in units of μK) can be written as

$$\langle T_{\text{line}} \rangle(z) = \frac{c^2}{2k_B \nu_{\text{obs}}^2} \int dM \frac{dn}{dM} \frac{L(M, z)}{4\pi \mathcal{D}_L^2} \left(\frac{dl}{d\theta} \right)^2 \frac{dl}{d\nu}, \quad (1)$$

where c is the speed of light, k_B is the Boltzmann factor, ν_{obs} is the observed frequency of the redshifted line,

dn/dM is the halo mass function, for which we adopt the Sheth-Tormen function [31]. $L(M, z)$ is the luminosity of CO- or [CII]-luminous galaxies (as a function of host-halo mass and redshift), and \mathcal{D}_L is the luminosity distance. The terms $dl/d\theta$ and $dl/d\nu$ reflect the conversion from units of comoving lengths, l , to those of specific intensity: frequency, ν , and angle, θ . The term $dl/d\theta$ is equivalent to comoving angular diameter distance, while $dl/d\nu = c(1+z)/[\nu_{\text{obs}}H(z)]$, where $H(z)$ is the Hubble parameter at a given redshift.

The power spectrum consists of two primary contributions: the clustering component (P_{clust}), which is sensitive to the distribution of objects and typically dominates on large scales, and the shot component (P_{shot} , sometimes referred to as the Poisson component), which arises due to the discrete nature of individual galaxies and dominates on small scales. On large scales, where clustering bias can be described by a linear relation, the clustering component can be expressed as $P_{\text{clust}}(k, z) = [b_{\text{line}}(z)]^2 b_{\text{line}}^2(z) P_0(k, z)$, where $P_0(k, z)$ is the linear matter power spectrum and $b_{\text{line}}(z)$ is the luminosity-weighted linear bias of the line emitting galaxy. This bias can be further written as

$$b_{\text{line}}(z) = \frac{\int dM \frac{dn}{dM} b_h(M, z) L(M, z)}{\int dM \frac{dn}{dM} L(M, z)}, \quad (2)$$

with $b_h(M, z)$ being the linear halo bias, for which we adopt prediction of Sheth-Tormen mass function. The shot component of the power spectrum takes the form of

$$P_{\text{shot}}(z) = \frac{c^4}{4k_B^2 \nu_{\text{obs}}^4} \int dM \frac{dn}{dM} \left[\frac{L(M, z)}{4\pi \mathcal{D}_L^2} \left(\frac{dl}{d\theta} \right)^2 \frac{dl}{d\nu} \right]^2. \quad (3)$$

Theory and current observational data suggest that both CO and [CII] exist in high-redshift galaxies ($z \gtrsim 6$) [32–34], and can therefore be used as tracers of the growth of structure in the early Universe. However, the strength of this emission is subject to a large uncertainty, and the predicted power spectrum is very sensitive to the astrophysical modeling. In our analysis presented here, we use the results of [35] to model the dependence of star formation rate on halo mass and redshift, and assume the luminosities of CO and [CII] can be written as a function of star formation rate, adopting the models of [36, 37].

There are two additional effects that we account for in modeling P_{clust} : redshift-space distortions [38, 39] and the Alcock-Paczynski (AP) effect [40, 41]. The former is due to the fact that the power spectrum is measured in redshift-space, where peculiar velocities of galaxies distort their distribution. The latter arises from the fact that one assumes a reference cosmology to infer distances from redshifts and angular position, which if incorrect, will distort the power spectrum measurement. The details of our modeling, including the impact of astrophysical modeling on our forecasts, are outlined in our accompanying paper [42].

Line bias from PNG: Local shape non-Gaussianity, leads to a distinct, scale-dependent correction to the linear halo bias [21–23]. Consequently, the line bias given in Eq. (2) receives a scale-dependent correction, $b_{\text{line}}(z) \rightarrow b_{\text{line}}(k, z) = b(z) + \Delta b_{\text{line}}^{\text{NG}}(k, z)$, the dominant contribution of which is given by

$$\Delta b_{\text{line}}^{\text{NG}}(k, z) = \frac{6}{5} \frac{f_{\text{NL}}^{\text{loc}} \delta_c [b_{\text{line}}(z) - 1]}{\mathcal{M}(k, z)}, \quad (4)$$

where $\delta_c = 1.686$ is the critical linear overdensity of spherical collapse at $z = 0$, and $\mathcal{M}(k, z)$ is the transfer function, relating the linear matter density fluctuations δ_0 to curvature perturbations, $\delta_0(\mathbf{k}, z) = \mathcal{M}(k, z)\zeta(\mathbf{k})$.

On larger scales, for $k \ll 0.02 \, h \, \text{Mpc}^{-1}$, the transfer function asymptotes to k^2 , producing a strong k^{-2} dependence in $\Delta b_{\text{line}}^{\text{NG}}$. Such a scale-dependence is unlikely to be caused by other astrophysical sources, therefore it provides a clean window to probe PNG of local shape. Over the next few years, LSS surveys will provide significantly improved constraints on $f_{\text{NL}}^{\text{loc}}$ by probing progressively larger volumes, utilizing the increasing strength of the signal at larger spatial scales (e.g., [19, 43–47]). Intensity mapping surveys can leverage this strategy by providing a relatively inexpensive method for accessing faint, distant objects at higher redshifts, and thus over larger volumes. With sufficient redshift coverage, even a survey covering a small fraction of the sky can probe the scales at which the enhancement in power from local PNG is significant.

Survey design and instrumental noise: For the intensity mapping of CO, we consider the J_{1-0} rotational transition (with rest-frame frequency of $\nu_{\text{rest}} = 115.271$ GHz), which we will refer to as CO(1-0). At the redshift range of interest, this transition is readily accessible to ground-based experiments. For our analysis, we consider a variant of the existing CO Mapping Array Pathfinder (COMAP) [36], which is currently designed to measure CO(1-0) at $z \sim 3$. This variant, which we will refer to as COMAP-Low, is a hypothetical future lower-frequency complement to the existing instrument, designed to perform a CO EoR intensity mapping experiments. With the exception of the frequency range, we generally adopt the existing parameters for COMAP as given in [36]. We consider an instrument utilizing 10-m aperture with 1000 dual-polarization detectors, with a spectral resolution of 30 MHz and coverage between [12–24] GHz, $z = [3.8 - 8.6]$. For this instrument, we assume that the system temperature of each element scales with frequency, such that $T_{\text{sys}} = \nu_{\text{obs}}$ (K/GHz) at frequencies above 20 GHz, and $T_{\text{sys}} = 20$ K below. We consider a survey covering 2000 sq. degrees, an area similar to that being surveyed by current 21 cm EoR instruments [48], with the instrument running at 50% duty-cycle for a period of 5 years, for a total integration time of $\tau_{\text{tot}} \approx 2 \times 10^4$ hours.

For the [CII] transition ($\nu_{\text{rest}} = 1900.539$ GHz), the limited transmission of the atmosphere at sub-mm wavelengths makes ground-based observations more challenging; we, therefore, consider a space-based instrument. The Primordial Inflation Explorer (PIXIE), designed to study inflation via polarized emission from the CMB [49], is ideal to probe [CII] emission from the redshift range of $z = [0.06 - 11.7]$ (the frequency range of 150–1800 GHz) [50]. PIXIE has frequency coverage between 30 GHz and 6 THz, with 400 15-GHz synthesized frequency channels provided by a Fourier transform spectrometer (FTS). Although relatively coarse at the lowest frequencies, such an instrument has adequate resolution for the redshift range of interest for [CII]. PIXIE is purpose-designed to conduct a full-sky CMB survey, but is suitable for wide-field [CII] intensity mapping studies. For our analysis, we limit consideration to the cleanest 75% of the sky (matching that of the proposed polarized CMB measurement).

For an intensity mapping analysis, the per-mode instrumental noise, P_N , is related to the per-voxel imaging sensitivity, σ_{vox} , by $P_N = \sigma_{\text{vox}}^2 V_{\text{vox}}$, where V_{vox} is the comoving volume contained within a single voxel. The per-voxel sensitivity depends on instrumental configuration. For an instrument like COMAP, $\sigma_{\text{vox}} = T_{\text{sys}} / \sqrt{\delta\nu \tau_{\text{int}}}$, where T_{sys} is the system temperature of the instrument, τ_{int} is the total integration time per single pointing and $\delta\nu$ is the frequency resolution for a single channel. Combining these two expressions, we can further define

$$P_N = \frac{T_{\text{sys}}^2}{\tau_{\text{tot}} N_{\text{det}}} \Omega_{\text{survey}} \left(\frac{dl}{d\theta} \right)^2 \frac{dl}{d\nu}, \quad (5)$$

where N_{det} is the number of detectors (i.e., single polarization feeds), and Ω_{survey} is the area of our survey.

For illustration, we show in Figure 1 the spherically averaged clustering contribution to the redshift-space line intensity power spectrum, $P_{\text{clust}}(k) = \int_{-1}^1 d\mu/2 P_{\text{clust}}(k, \mu)$, for CO and [CII], accounting for the AP effect and in the presence of PNG with $f_{\text{NL}}^{\text{loc}} = 6.5$. The expected spherically averaged variance is shown as shaded blue region and is given by [51],

$$\frac{1}{\sigma_P^2(k)} = \sum_{\mu} \frac{k^3 V_{\text{survey}}}{8\pi^2} \frac{\Delta\mu}{\text{var}[P(k, \mu)]}, \quad (6)$$

where μ is the cosine of the angle with respect to the line of sight and $\text{var}[P(k, \mu)] = [P_{\text{clust}}(k, \mu) + P_{\text{shot}}(k) + \tilde{P}_N(k, \mu)]^2$. Here $\tilde{P}_N(k, \mu) = P_N e^{(k_{\parallel}/k_{\parallel, \text{res}})^2 + (k_{\perp}/k_{\perp, \text{res}})^2}$, where $k_{\parallel} = k\mu$ and $k_{\perp}^2 = k^2 - k_{\parallel}^2$ are the components of the wavenumber parallel and perpendicular to the line of sight and $k_{\parallel, \text{res}}$ and $k_{\perp, \text{res}}$ represent the finite resolution of the survey in the two directions. We adopt logarithmic bins of width $\epsilon = d \ln k$. For illustration, we also show the shot (dotted red) and the clustering components of the power spectrum with

Gaussian initial conditions (dashed-dotted purple). The vertical lines correspond to the smallest scale k_{max} , that we consider in our forecast. For [CII], due to limited resolution of PIXIE, the value of k_{max} is generally set by the angular resolution ($\theta = 1.6^\circ$) at high redshift, and frequency resolution ($\delta\nu = 15$ GHz) at low redshift. For CO, we choose $k_{\text{max}} = 0.15 h \text{ Mpc}^{-1}$ at redshift zero, while at other redshifts we set it such that the variance of the density field at that redshift is the same as $z = 0$, and further impose a conservative bound of $k_{\text{max}} < 0.3 h \text{ Mpc}^{-1}$ to assure the validity of assumptions of linear bias.

Fisher forecast: We perform a Fisher matrix analysis to forecast the potential of the CO(1-0) and [CII] intensity mapping surveys to constrain PNG. In our forecast, we vary the amplitude of local PNG, setting its fiducial value to $f_{\text{NL}}^{\text{loc}} = 1$. Additionally, we vary five cosmological parameters, namely the amplitude and the spectral index of primordial fluctuations, the Hubble parameter, and the energy density of cold dark matter and baryons with the fiducial values set to best-fit parameters from Planck 2015 [52]. We also vary the velocity dispersion (which affects the modeling of redshift-space distortions) with the fiducial value set to $\sigma_{\text{FOG}, 0} = 250 \text{ km s}^{-1}$. Instead of varying the bias as a free parameter, we assume that it is given by Eq. (2), which has a dependence on cosmological parameters. We bin each survey into redshift bins of approximate width $\log_{10}[\Delta(1+z)] = 0.1$.

Results: Using the entire available three-dimensional volume, we find that a PIXIE- and COMAP-like experiments are capable of reaching 68% C.L. of $\sigma(f_{\text{NL}}^{\text{loc}}) = 4.9$ and $\sigma(f_{\text{NL}}^{\text{loc}}) = 3.7$ respectively, imposing Planck priors on cosmological parameters. The strength of the constraints on local shape PNG from each survey is determined by two factors: largest scales accessible, and per-mode noise of the instrument. For PIXIE, the strongest constraints arise from $z \lesssim 3$; above this redshift, the increasing per-mode noise overtakes the enhancement in power from PNG at low k . In contrast, the increased per-mode sensitivity of COMAP-Low provide relatively even constraints on $\sigma(f_{\text{NL}}^{\text{loc}})$ across all redshift bins. While limited in sky coverage, the ability of COMAP-Low to probe the cosmic web at higher redshifts provides access to the large volumes – and corresponding large scale-modes – required for constraining $f_{\text{NL}}^{\text{loc}}$.

In the analysis presented here, we note that we have assumed that foregrounds, interloper lines and systematic errors are well constrained, and not a limiting factor in our analysis. Experiments targeting CO and [CII] are likely to benefit from decades of work in continuum foreground modeling that have been performed as part of CMB surveys, although instrumental errors may limit the fidelity with which these foregrounds can be removed, inducing scale-dependent foreground contributions to a power spectrum measurement [50]. The removal of interloper line emission is presently an area of

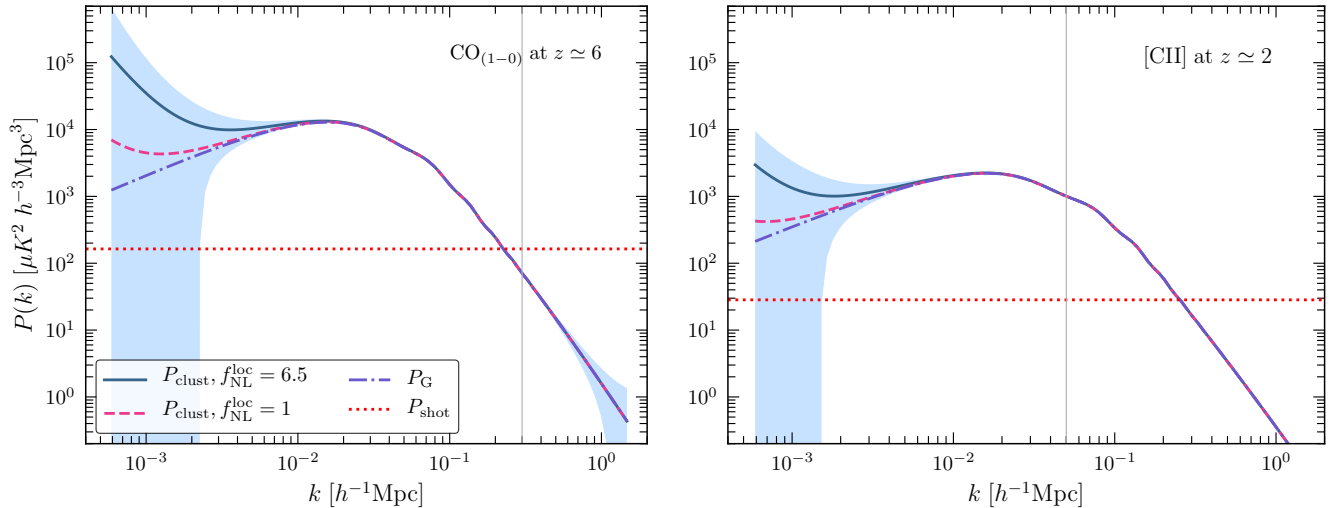


FIG. 1: The spherically averaged clustering component of the power spectrum (including AP effect) for $f_{\text{NL}}^{\text{loc}} = 6.5$ (solid blue) and $f_{\text{NL}}^{\text{loc}} = 1$ (dashed magenta) for CO(1-0) at $z \simeq 6$ (left) and [CII] (right) at $z \simeq 2$ are shown. These redshifts are chosen since for the experiments considered here, they provide the tightest constraints on $f_{\text{NL}}^{\text{loc}}$. The shaded blue region is the expected spherically averaged variance for the power spectrum with $f_{\text{NL}}^{\text{loc}} = 6.5$, defined in Eq. (6). For illustration we also show the spherically averaged Gaussian contribution (dashed-dotted purple), as well as the shot contribution (dotted red). The vertical lines correspond to the smallest scale k_{max} considered in our forecast, the choice of which is described in the text.

active development. For CO, the contribution of interloper lines is likely to be negligible [53]. However, lower redshift CO emission (from several rotational transitions of the molecule) could represent a significant foreground for [CII]. Existing theoretical work suggests a variety of methods for removing or reducing the impact of spectral foregrounds (e.g., [54, 55]). We note that this contamination is likely to be most significant for $z \geq 6$, where PIXIE provides limited constraints. This potential contamination is therefore unlikely to affect the results presented here, although it may represent a limitation for other EoR-targeted experiments seeking to constrain $f_{\text{NL}}^{\text{loc}}$. A more detailed exploration of the impact of systematics and foregrounds can be found in our accompanying paper [42].

Conclusions: The proposed CO(1-0) and [CII] surveys can achieve 68% C.L. of $\sigma(f_{\text{NL}}^{\text{loc}}) = 3.7$ and $\sigma(f_{\text{NL}}^{\text{loc}}) = 4.9$. The constraints from COMAP-Low and PIXIE, are an improvement on those from Planck, and are comparable to those from measurements of power spectrum from upcoming galaxy surveys such as EUCLID [56] ($\sigma(f_{\text{NL}}^{\text{loc}}) = 3.9$ [57]), DESI [58] ($\sigma(f_{\text{NL}}^{\text{loc}}) = 4.8$ [45]) and LSST [59] ($\sigma(f_{\text{NL}}^{\text{loc}}) = 1.4$ [57]).

We note that our analysis has focused on instruments with present prototypes or existing designs that would be capable of probing primordial non-Gaussianity via CO and [CII] intensity mapping, rather than hypothetical instruments optimized to do so. As such, there is significant potential for a more optimized experiment to probe the distribution of matter at large scales and high redshifts via [CII] and CO intensity mapping, offering a promising

window to constrain primordial non-Gaussianity. This potential is bolstered by the highly complementary requirements between a PNG-focused intensity mapping survey – in terms of resolution, frequency coverage, survey area, and sensitivity – and select future surveys targeting CMB and EoR-related science. At the cosmic variance limit, an EoR-focused ($z = [6 - 10]$) intensity mapping survey targeting CO or [CII] would achieve $\sigma(f_{\text{NL}}^{\text{loc}}) \approx 0.3$, suggesting that a ground-based experiment with limited sky-coverage may be capable of significantly improving constraints on f_{NL} .

Prospects: Given the unique potential of intensity mapping with emission lines in constraining PNG, understanding the dependence of the constraints on astrophysical modeling is critically important. Equally important are more detailed studies of the impact of foregrounds and systematics, particularly on the large-scale modes which are essential in constraining local PNG from power spectrum measurements. We give further consideration of this and the study of optimal experimental set up, best-fit to probe PNG with intensity mapping, in our accompanying work [42]. Finally, the multi-tracer technique can further improve our results by minimizing the cosmic variance noise [61]. For [CII] intensity mapping with PIXIE, multi-tracer analysis is particularly timely since the range of redshifts that provide the most constraining power is well-matched to several of the aforementioned galaxy surveys. We defer the study of the potential of multi-tracer technique with intensity mapping surveys to future work.

Acknowledgment: It is our pleasure to thank Tzu-Ching Chang, Olivier Doré, and Eric Switzer for fruitful discussion and helpful comments on this manuscript. We further thank Eric Switzer for providing us the updated PIXIE noise curves and Julian Muñoz for providing us the Planck Fisher matrix used to obtain Planck priors.

* Electronic address: amoradinejad@fas.harvard.edu

- [1] A. H. Guth, Phys. Rev. **D23**, 347 (1981).
- [2] A. D. Linde, Phys. Lett. **108B**, 389 (1982).
- [3] A. Albrecht and P. J. Steinhardt, Phys. Rev. Lett. **48**, 1220 (1982).
- [4] V. F. Mukhanov and G. V. Chibisov, JETP Lett. **33**, 532 (1981), [Pisma Zh. Eksp. Teor. Fiz.33,549(1981)].
- [5] A. A. Starobinsky, Phys. Lett. **117B**, 175 (1982).
- [6] S. W. Hawking, Phys. Lett. **115B**, 295 (1982).
- [7] A. H. Guth and S. Y. Pi, Phys. Rev. Lett. **49**, 1110 (1982).
- [8] T. J. Allen, B. Grinstein, and M. B. Wise, Phys. Lett. **B197**, 66 (1987).
- [9] T. Falk, R. Rangarajan, and M. Srednicki, Phys. Rev. **D46**, 4232 (1992), astro-ph/9208002.
- [10] A. Gangui, F. Lucchin, S. Matarrese, and S. Mollerach, Astrophys. J. **430**, 447 (1994), astro-ph/9312033.
- [11] N. Bartolo, E. Komatsu, S. Matarrese, and A. Riotto, Phys. Rept. **402**, 103 (2004), astro-ph/0406398.
- [12] X. Chen, Adv. Astron. **2010**, 638979 (2010), 1002.1416.
- [13] L.-M. Wang and M. Kamionkowski, Phys. Rev. **D61**, 063504 (2000), astro-ph/9907431.
- [14] L. Verde, L.-M. Wang, A. Heavens, and M. Kamionkowski, Mon. Not. Roy. Astron. Soc. **313**, L141 (2000), astro-ph/9906301.
- [15] E. Komatsu and D. N. Spergel, Phys. Rev. **D63**, 063002 (2001), astro-ph/0005036.
- [16] J. M. Maldacena, JHEP **05**, 013 (2003), astro-ph/0210603.
- [17] P. Creminelli and M. Zaldarriaga, JCAP **0410**, 006 (2004), astro-ph/0407059.
- [18] Planck, P. A. R. Ade et al., Astron. Astrophys. **594**, A17 (2016), 1502.01592.
- [19] S. Camera, M. G. Santos, and R. Maartens, Mon. Not. Roy. Astron. Soc. **448**, 1035 (2015), 1409.8286.
- [20] M. Alvarez et al., (2014), 1412.4671.
- [21] N. Dalal, O. Dore, D. Huterer, and A. Shirokov, Phys. Rev. **D77**, 123514 (2008), 0710.4560.
- [22] S. Matarrese and L. Verde, Astrophys. J. **677**, L77 (2008), 0801.4826.
- [23] N. Afshordi and A. J. Tolley, Phys. Rev. **D78**, 123507 (2008), 0806.1046.
- [24] S. Camera, M. G. Santos, P. G. Ferreira, and L. Ferramacho, Phys. Rev. Lett. **111**, 171302 (2013), 1305.6928.
- [25] G. K. Keating et al., Astrophys. J. **830**, 34 (2016), 1605.03971.
- [26] A. R. Pullen, P. Serra, T.-C. Chang, O. Dore, and S. Ho, ArXiv e-prints (2017), 1707.06172.
- [27] E. D. Kovetz et al., (2017), 1709.09066.
- [28] C. Carilli and F. Walter, Ann. Rev. Astron. Astrophys. **51**, 105 (2013), 1301.0371.
- [29] L. J. Tacconi et al., Astrophys. J. **768**, 74 (2013), 1211.5743.
- [30] R. Herrera-Camus et al., Astrophys. J. **800**, 1 (2015), 1409.7123.
- [31] R. K. Sheth and G. Tormen, Mon. Not. Roy. Astron. Soc. **308**, 119 (1999), astro-ph/9901122.
- [32] B. P. Venemans et al., Astrophys. J. **816**, 37 (2016), 1511.07432.
- [33] B. Venemans et al., Astrophys. J. **845**, 154 (2017), 1707.05238.
- [34] G. Popping et al., MNRAS **461**, 93 (2016), 1602.02761.
- [35] P. S. Behroozi, R. H. Wechsler, and C. Conroy, Astrophys. J. **770**, 57 (2013), 1207.6105.
- [36] T. Y. Li, R. H. Wechsler, K. Devaraj, and S. E. Church, Astrophys. J. **817**, 169 (2016), 1503.08833.
- [37] M. B. Silva, M. G. Santos, A. Cooray, and Y. Gong, Astrophys. J. **806**, 209 (2015), 1410.4808.
- [38] N. Kaiser, Mon. Not. Roy. Astron. Soc. **227**, 1 (1987).
- [39] J. C. Jackson, Mon. Not. Roy. Astron. Soc. **156**, 1P (1972), 0810.3908.
- [40] C. Alcock and B. Paczynski, Nature **281**, 358 (1979).
- [41] W. E. Ballinger, J. A. Peacock, and A. F. Heavens, Mon. Not. Roy. Astron. Soc. **282**, 877 (1996), astro-ph/9605017.
- [42] A. Moradinezhad Dizgah, G. K. Keating, and A. Fialkov, in prep., (2018)
- [43] T. Giannantonio, C. Porciani, J. Carron, A. Amara, and A. Pillepich, Mon. Not. Roy. Astron. Soc. **422**, 2854 (2012), 1109.0958.
- [44] R. de Putter and O. Dor, Phys. Rev. **D95**, 123513 (2017), 1412.3854.
- [45] S. Gariazzo, L. Lopez-Honorez, and O. Mena, Phys. Rev. **D92**, 063510 (2015), 1506.05251.
- [46] D. Alonso, P. Bull, P. G. Ferreira, R. Maartens, and M. Santos, Astrophys. J. **814**, 145 (2015), 1505.07596.
- [47] M. Tucci, V. Desjacques, and M. Kunz, Mon. Not. Roy. Astron. Soc. **463**, 2046 (2016), 1606.02323.
- [48] D. R. DeBoer et al., PASP **129**, 045001 (2017), 1606.07473.
- [49] A. Kogut et al., JCAP **7**, 025 (2011), 1105.2044.
- [50] E. R. Switzer, Astrophys. J. **838**, 82 (2017), 1703.07832.
- [51] A. Lidz et al., Astrophys. J. **741**, 70 (2011), 1104.4800.
- [52] Planck, P. A. R. Ade et al., Astron. Astrophys. **594**, A13 (2016), 1502.01589.
- [53] D. T. Chung, T. Y. Li, M. P. Viero, S. E. Church, and R. H. Wechsler, (2017), 1706.03005.
- [54] A. Lidz and J. Taylor, Astrophys. J. **825**, 143 (2016), 1604.05737.
- [55] Y.-T. Cheng, T.-C. Chang, J. Bock, C. M. Bradford, and A. Cooray, Astrophys. J. **832**, 165 (2016), 1604.07833.
- [56] L. Amendola et al., (2016), 1606.00180.
- [57] A. Moradinezhad Dizgah and C. Dvorkin, (2017), 1708.06473.
- [58] DESI, A. Aghamousa et al., (2016), 1611.00036.
- [59] LSST Science, LSST Project, P. A. Abell et al., (2009), 0912.0201.
- [60] O. Dor et al., (2014), 1412.4872.
- [61] U. Seljak, Phys. Rev. Lett. **102**, 021302 (2009), 0807.1770.